Control of Pore Structure Formation in Cellulose Nitrate Polymer Membranes

Eoin J. Flynn, Jovanna Arndt, Léa Brothier, Michael A. Morris*

[a]Chemistry Department, University College Cork, Cork, Ireland
[b]Environmental Research Institute ,University College Cork, Lee Road, Cork, Ireland

*Corresponding Author: Michael A. Morris (m.morris@ucc.ie) Tel: 00-353-21-490-2180

Abstract

Porous cellulose based membranes are commonly used for filtration and controlled flow of fluid through the 3D pore network in the bulk (lateral flow). It has been shown that the performance of *cellulose nitrate* membranes in terms of capillary driven lateral flow of fluid through the system is inhibited by the formation of surface skin layers and bulk macrovoids. These 'defects' are created during phase inversion when the porous structure is formed using a water anti-solvent. The work carried out in this study shows that the incorporation of ethanol as a *meso-solvent* into the membrane casting solution for use in *vapour induced phase seaparation* (VIPS) produced lateral flow membranes, effectively prevents the formation of both skin layers and macrovoids while simultaneously increasing membrane porosity resulting in an improvement in lateral flow rates of the final membranes. It is indicated that the improved performance is achieved through reduction of the rate of evaporation of solvent from the membrane surface/demixing front during membrane formation.

Keywords

Ethanol; Lateral-Flow; Cellulose-Nitrate; Macrovoid; Skin-Layer

Introduction

Porous, lateral-flow, polymer membranes are the basis for the vast majority of immunological and diagnostic assays. Cellulose derived polymers are most commonly used for the production of lateral flow membranes. In particular, cellulose nitrate (CN, often referred to by the misnomer *nitrocellulose*) is very widely used.(Ulbricht 2006; Lönnberg & Carlsson 2001; Ahmad et al. 2007) However, despite widespread use, there has been relatively little investigation into the formation of cellulose nitrate lateral flow membranes in literature.

These porous membranes are formed through a process known as *phase inversion* which defines their internal pore structure.(Yip & Mchugh 2006; Vandewitte et al. 1996; B. F. Barton et al. 1997) This is a phenomenon whereby the phases of a liquid-liquid dispersion interchange such that the dispersed phase spontaneously inverts to become the continuous phase and vice versa under conditions determined by the system properties, volume ratio and energy input.(Arirachakaran et al. 1989) The phase inversion method utilised here is vapour induced phase inversion (VIPS)(Chae et al. 1999) wherein diffusion of water from atmospheric humidity into the polymer solution of CN in acetone induces demixing of the polymer from the solution to form the solid porous CN matrix of the final membrane. When a polymer solution is in a single phase the polymer is stable in the solvent. The addition of nonsolvent (water) decreases the thermodynamic stability of the solution as its concentration relative to the solvent (acetone) decreases. At a critical concentration (*cloud point*) of nonsolvent, the solution becomes thermodynamically unstable and two liquid phases – a polymer rich phase, containing solvent and polymer, and a polymer lean phase containing the non-solvent - are formed. Upon drying, the polymer rich phase forms the rigid matrix of the membrane while the polymer lean phase forms the pores.(Kang et al. 1988) Evaporative loss of solvent precipitates the final membrane morphology.(Salamone 1996) Phase inversion is a sensitive process and can be affected by many parameters; solution concentration, viscosity, surface tension, density, temperature, humidity, container geometry, agitation and flow.(Hu et al. 2006) The sparse literature on CN membranes (and membranes produced by phase inversion in general) consistently shows the formation of skin layers(Ahmad et al. 2005; Ahmad et al. 2008; Kang et al. 1988; T.-H. Young & L.-W. Chen 1995; Kim & Lee 1998) and macrovoids (Ahmad et al. 2007; Khare et al. 2002; Smolders et al. 1992; Paulsen et al. 1994) in the membrane cross sections. While methods to prevent macrovoid formation during the phase inversion process have been documented and studied in detail[3,14], prevention of the formation of skin layers has not.

Skin layers and macrovoids inhibit and retard lateral flow in porous membranes respectively, limiting their

properties and use. The work in this study shows how the formation of both skin layers and macrovoids can be successfully prevented through the use of an additional solvent that has solvating properties somewhere between the solvent and non-solvent used in preparation. This additional solvent (which is described here as the *meso-solvent*) is also partially miscible with both the solvent and the non-solvent. In this case, ethanol is the meso-solvent to the basic phase inversion make-up of polymer (CN), solvent (acetone) and non-solvent (water). The use of ethanol as a meso-solvent increases the porosity of the membrane internal structures, which also results in an increase in lateral flow rates through the membranes.

Ethanol has been used as a quencher in the casting of similar membranes,(Hao & Wang 2001) but this role is distinct from the meso-solvent role and, in addition, it was found to be inferior to methanol as a quencher. To the best of our knowledge, the use of ethanol as a meso-solvent in the production of membranes of the type herein has not been covered in the literature and is presented here for scientific posterity.

Experimental

Materials

The cellulose nitrate polymer used is crystalline in nature with an average polydispersity (Mw/Mn) of 2.681, where Mw/Mn are the weight average molecular weight/and the number average molecular weight respectively. 100% polyester film was used as a membrane support. Surfactants including sodium C10-15 sulphate, sodium C10-15 benzene sulphate, sodium C14-17 sec-Alkyl sulphonate, sodium C10-15 ether sulphate and sodium stearate were used to render the final membrane hydrophilic. Chemicals were purchased from Sigma-Aldrich Chemie Gmbh, Germany and were used without further purification.

Apparatus

An automatic film applicator (model K202 Control Coater produced by RK Printcoat Instruments Ltd., UK) was used for membrane casting. All membranes were cast onto 100 μm thickness 100% polyester film attached to 25 cm^2 glass plates and subsequently removed. It was important for membrane synthesis reproducibility that humidity was carefully controlled. For this purpose, all membrane were cast and phase inverted inside an MBraun GP 2202 PB single piece moulded glovebox, supplied by MBraun UK, Ltd. The humidity was maintained at 35%.

Membrane Preparation

A series of membranes were produced from casting solutions. The content of these solutions can be seen in table 1 below. The solvent/ meso-solvent/ non-solvent mixture for each casting solution contained differing amounts of ethanol and acetone with a constant water content (prior to addition of extra non-solvent to make solution near cloud point), ranging from 25wt% ethanol/70wt% acetone/5wt% water to 50wt% ethanol/45wt% acetone/5wt% water. Outside this composition range, membranes were either highly irreproducible or had poor physical properties in terms of fragility, pore structure, porosity and skin formation. 83g of each of these solutions was used to dissolve 17 g of CN. 20g aliquots of the resulting solutions (or lacquers) were then brought to near cloud point by incorporating additional non-solvent - water - and the weight percentages of the polymer solutions were calculated as shown in the right side of table 1. Although it has previously been shown that near cloud-point compositions lead to instantaneous skin formation(Pesek & W.J. Koros 1993), the inclusion of ethanol as a meso-solvent negates this effect for reasons outlined below, allowing for casting and formation of membranes without skin layers. The membranes in this series are labelled A – E; A being that with the lowest ethanol content and E being that with the highest. These membranes were then compared with one produced using a simple solvent/non-solvent solution of 95wt% acetone and 5wt% water in which 17g CN was dissolved to provide a membrane produced from a more typical phase inversion without a meso-solvent. 2.3g of water were added to bring this solution to near cloud point. The weight percentage composition can be seen in the final row of table 1. This control membrane was labelled F. Final membranes were produced with backing supports of the 100% polyester film by casting the near cloud point polymer solutions on to the support material using the automatic film coater. This cast layer underwent VIPS in the controlled glovebox atmosphere at 35% humidity and ~24°C and remained in this environment for 12hrs. Finally, the resulting membrane was dried at 30°C for approximately 4hrs to remove excess solvent/ meso-solvent/ non-solvent before characterization.

Table 1: Casting solution composition before/after cloud point (abbreviations: Mem. = membrane; poly. = polymer; sol. = solvent; CP = cloud point; PI = phase inversion)

Mem.	Initial PI Solution				Non-sol. (H_2O) for near CP (g)	Solution Near CP			
	Poly. (CN) wt %	Sol. (ace.) wt %	Meso-sol. (EtOH) wt%	Non-sol. (H_2O) wt %		Poly. (CN) wt %	Sol. (ace.) wt %	Meso-sol. (EtOH) wt%	Non-sol. (H_2O) wt %
A	17	58.10	20.75	4.15	5.30	13.03	44.53	15.90	26.53
B	17	53.95	24.90	4.15	5.43	12.89	40.90	18.88	27.33
C	17	49.80	29.05	4.15	5.55	12.80	37.50	21.87	27.83
D	17	45.65	33.20	4.15	5.94	12.57	33.74	24.54	29.15
E	17	41.50	37.35	4.15	4.80	13.22	32.27	29.04	25.47
F	17	78.85	0	4.15	2.30	15.12	70.14	0	14.73

Membrane Characterization

The morphologies of the cross sections and top surfaces of the membranes were characterised using a JEOL model FEI FP 2031/11 Inspect F field emission scanning electron microscope. All images of membranes were obtained under similar resolutions. All membrane samples were prepared for imaging by Cryo-Rupturing Image Sample Preparation (CRISP)(Flynn et al. 2012) method, to preserve internal structure. All polymer membrane samples required gold-coating to provide a conductive surface to allow imaging. All gold coatings were approximately 45nm thickness. Porosimetry was conducted using mercury porosimeter model Micromeritics AutoPore IV 9500 V1.09. Membranes were removed from polyester support material for porosimetry tests. Membrane crystallinity was determined by X-ray powder diffraction using a Philips X'Pert MPD Pro diffractometer with Cu Kα radiation 1.540598Å, utilizing Panalytical X'Pert data collector and X'Pert Highscore.

Lateral Flow Testing

Membrane lateral flow speeds were determined by testing capillary flow rates of water through the membranes. Membranes were cut into 120mm x 280mm strips. A horizontal line was drawn 15 mm from the bottom; a second line was drawn 15 mm from the top; giving a region 250 mm in length between. The membrane strip was then placed vertically in a 10 mm depth of water. The water flow was timed between the two marks and a flow speed was determined to give the lateral flow rates. The cellulose nitrate polymer was inherently hydrophobic and little or no flow was observed. In order to render it hydrophilic it was treated with surfactant. This was achieved by placing the membrane in solutions of 0.1wt% of SDBS surfactant in deionised water for 20 mins, followed by drying the membrane at room temperature. Subsequent SEM images of surfactant on the membrane surfaces (images available upon request) and bestowment of hydrophilicity upon the membrane confirmed the presence and effect of the surfactant treatment. This form of lateral flow test is an industrial SOP making results directly comparable with the stated flow rates of industrial membranes. The effect of gravity on the flow rate is constant for all membranes so the relative differences in flow between membranes serves to show improvement resulting from changes in membrane structure.

Results

Figure 1 shows a graph of the required additional non-solvent (water) to make the casting solutions near cloud-point versus their ethanol content. It can be seen from this that there is an increase in the amount of water required as ethanol content increases up to a maximum, beyond which the amount of water required decreases. The Hildebrand solubility parameters of acetone, ethanol and water are 19, 26.2 and 48 $MPa^{1/2}$ respectively, whilst CN is around 22 $MPa^{1/2}$ (A. F. M. Barton 1990) The maximum observed in figure one as the water required to achieve cloud point, can be explained on the basis of these. As ethanol concentration increases, hydrogen bonding with water reduces the anti-solvent properties of the water, thus requiring increased water concentrations. At higher ethanol content, the reduced amount of acetone has a more pronounced effect and the solubility of the CN decreases (since acetone is an effective solvent for CN).

Temperature affects the lacquer and higher temperatures increase the amount of non-solvent required to bring the solution to cloud point (as increased temperature increases the solubility of the

polymer in the solvent). At lower temperatures, the opposite is the case, less non-solvent is required to achieve phase inversion. This is the basic of TIPS (temperature induced phase inversion)

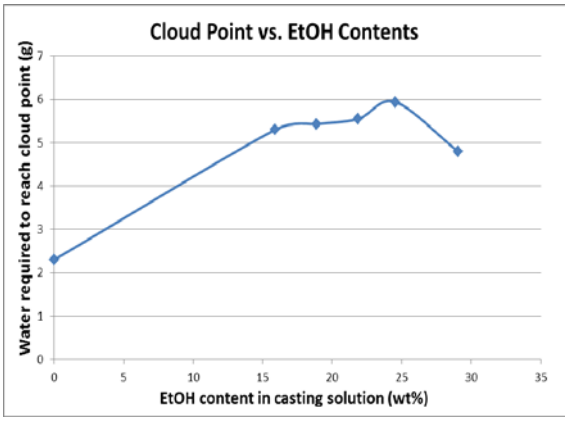

FIG. 1 PLOT OF NON-SOLVENT (WATER) REQUIRED TO REACH CLOUD POINT VERSUS ETHANOL CONTENT IN CASTING SOLUTION AT CLOUD POINT

Fig. 2, below, shows SEM images of the membranes A – F as labelled in the figure. Each pair is composed of a cross sectional membrane image (i) and an exposed membrane surface image (ii). Images F(i) and F(ii) show cross sectional and surface images respectively of membrane F, which has no ethanol in its casting solution. The cross section indicates some porosity but this is limited and there is little sign of pores extended in the direction normal to the membrane surface. What pores are visible appear to be largely 1D or 2D in nature and sandwiched between layers of CN. Although bringing solutions near to cloud-point prior to casting is thought to reduce skin layer formation by some,[18] (and refuted by others(Pesek & W.J. Koros 1993)) a well-formed skin layer is clearly visible in the top-down image shown in figure 2F(ii). There is little indication of open pores at the membrane surface although circular type features can be seen in either surface indentations or sub-surface structures. The observation of these is consistent with the formation of a closed 2D pore structure in the film. The layered nature of CN and the pore structure are suggested to be due to rapid solvent evaporation during casting as the solvent moves too rapidly through the membrane to allow 3D formation of pores.(Yiotis, Tsimpanogiannis, Stubos & Yortsos 2006a)

Images figure 2A(i) and 2A(ii) show membrane A which has the lowest meso-solvent (ethanol) content of 15.902wt% in its casting solution (Table 1). The cross sectional image, A(i), still indicates distinct layer formation consistent with a high rate of solvent evaporation. Again some inter-layer porosity is present. However, the presence of the ethanol has begun to evolve a new form of 3D pore structure that extends through the layers. This is largely seen as smaller pores around 1 to 5 μm in size. These are marked with rings and visible in both cross-section and top-down images (through much larger pore openings). These small pores seen in the surface are highly distorted into elliptical shapes and indicate considerable strain at the surface during membrane formation. The surface image, A(ii), also shows the formation of a 3D pore structure with very large pore openings of approximately 100 μm in diameter. It has been suggested that the large surface morphologies are formed because of the same surface tension effects described above are causing some of these pores to be deformed.(Pauchard & Allain 2003)

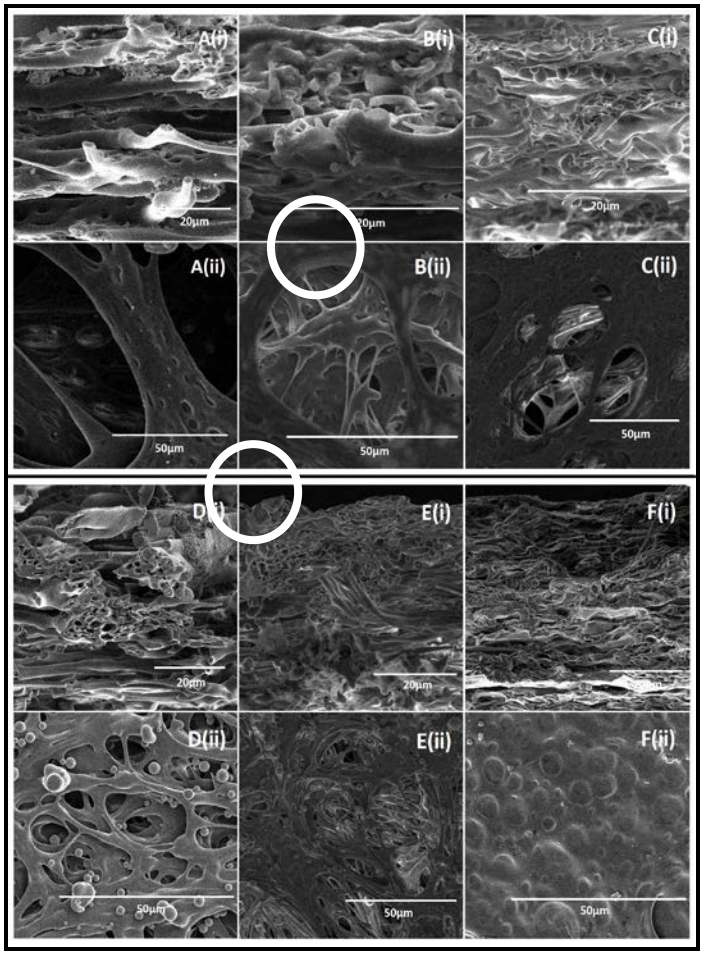

FIG. 2 SEM IMAGES OF THE LATERAL FLOW MEMBRANES A – F (LETTERING FOLLOWS SAMPLE LABELS SEE TABLE 1). IMAGES WITH THE (i) LABELS SHOW MEMBRANE CROSS SECTIONAL MORPHOLOGY WHILE THOSE WITH LABEL (ii) SHOW MEMBRANE SURFACE MORPHOLOGY.

Images in figure 2 B(i) and B(ii) show cross sectional and surface images respectively of membrane B, which has an ethanol content of ~18.9wt% in its casting solution (~3wt% more than membrane A). The cross

sectional image shows a structure similar to that observed in membrane A, however, there is a less distinctive layered structure, void formation and interconnectivity between layers is increasing. This might suggest that the ethanol decreases the rate of membrane formation (through reduction in the solvent evaporation rate) allowing more pore volume to be included. The interconnectivity of the layers and the progression of a 1D or 2D pore structure into a 3D pore arrangement can be clearly seen in the top-down surface image, in figure 2B(ii). Note that the size of the openings at the surface morphologies is significantly reduced to about 60 μm compared to similar features seen in membrane A. This is consistent with lower evaporation rate which would allow some of the surface strain to be reduced during membrane formation. The smaller pores seen for membrane A are also observed around the same size but, as it might be expected, they are significantly less strained and distorted at the surface.

Increasing the ethanol further to around 22wt% (membrane C) continues the trend seen for membranes discussed so far. Images shown in figures 2C(i) and C(ii) show cross sectional and surface images respectively. The formation of a layered structure is barely observable and the pore volume is clearly increasing. It is clear that the films membranes formed by this methodology will always have significant layered structure probably because of the way in which the solvent from moves through the film during drying. Noticeable also is the appearance of quite large spherical structures or nodules suggestive of some nucleation and growth which is consistent with lower rates of membrane formation. The smaller pores can be seen quite clearly in both top-down and cross-section images but it should be noted that at the surface the pores are largely undistorted, consistent with low strain resulting from lower rates of membrane formation.

Images figure 2D(i) and D(ii) show cross sectional and surface images respectively of membrane D, which has an ethanol content of about 25wt% in its casting solution. The trends in morphologies observed in membranes A-C continue in membrane D. The cross section, image figure 2D(i), still shows indications of layering but the layering appears to be very much 1D and filamental in form. This is because there are large pore opening in the layers, as seen quite clearly in the corresponding top-down SEM (figure 2D(ii)). Quite clear void formation between the layers and the small pores of (1-5 μm) can not only be seen as existing through the layers but within the material as well. It is apparent that this is the most porous of the membranes seen thus far. The top-down surface image, figure 2D(ii) reveals the 3D nature of the open porous structure formed although their size is reduced a little compared to membrane C to an approximate diameter of 25 μm. The size and shape are consistent with continued slower membrane formation and strain release. While no nodules are observed in cross section, they are present in the surface image.

Images in figure 2E(i) and E(ii) detail the morphology of membrane E (about 29wt% ethanol). The morphology of the membrane is quite close to that of membrane D in all respects and is observed in both cross-section and top-down images. The only difference is increased density and lower void volume. This can be particularly seen in the upper region of the membrane in figure 2E(i). The data, thus, suggest that membrane D is probably the most porous of those studied.

In order to reveal these changes in the membrane further, membrane D and membrane F have been studied to assess and compare the non-ethanol containing solvent and the most porous of the meso-solvent modified membranes. Figure 3 shows XRD data for the membranes. A large broad feature around 22-32$^{o}2\theta$ and weaker features around 45 and 65$^{o}2\theta$ are consistent with a poorly ordered crystalline material and the features are similar for both membranes.(Thurn-Albrecht et al. 2004) However, the membrane D material also shows sharp diffraction features at 29.34$^{o}2\theta$ and 32.58$^{o}2\theta$ (as highlighted in the figure). These are consistent with the presence of highly crystalline material as well as a majority of the poorly defined phase. Due to the increased presence of nodules seen in the SEM images as nodules are a crystalline morphology.(Stevens 1999; Van-de-Witte 1996) The data represent evidence that increasing the membrane casting solution ethanol content increases the final membrane crystallinity and has a very direct effect on the kinetics of membrane formation. Increased crystallinity is consistent with longer membrane formation times which allow structural refinement during synthesis.

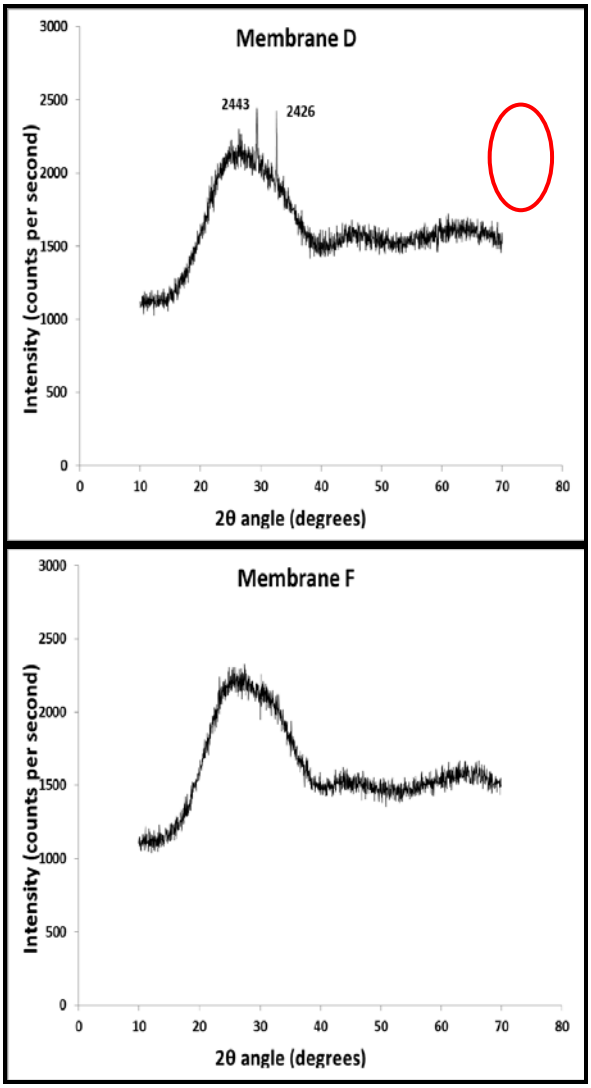

FIG. 3 XRD PROFILES OF MEMBRANE D AND MEMBRANE F

To confirm the image analysis, mercury porosimetry data were recorded from membranes D and F in figure 4. BET testing was conducted using nitrogen and even argon gases. However, it was found that the membranes retain too much gas to give an accurate measurement, leaving mercury porosimetry as the only viable accurate means to obtain porosity data. Figure 4A shows the cumulative intrusion of mercury in the membrane versus pressure and the data clearly show that membrane D has a greater overall internal volume than that of membrane F in agreement with the SEM analysis. Figure 4B shows the log differential of mercury intrusion into the membrane versus pore size diameter. The data shows that the ethanol meso-solvent increases the number of large pores (i.e. >10 μm) within the membrane. The data also indicate a well-defined peak below 10 μm which is consistent with the smaller pores seen in the SEM data from samples made with ethanol included. Again all data are consistent with the analysis of the SEM images in figure 2.

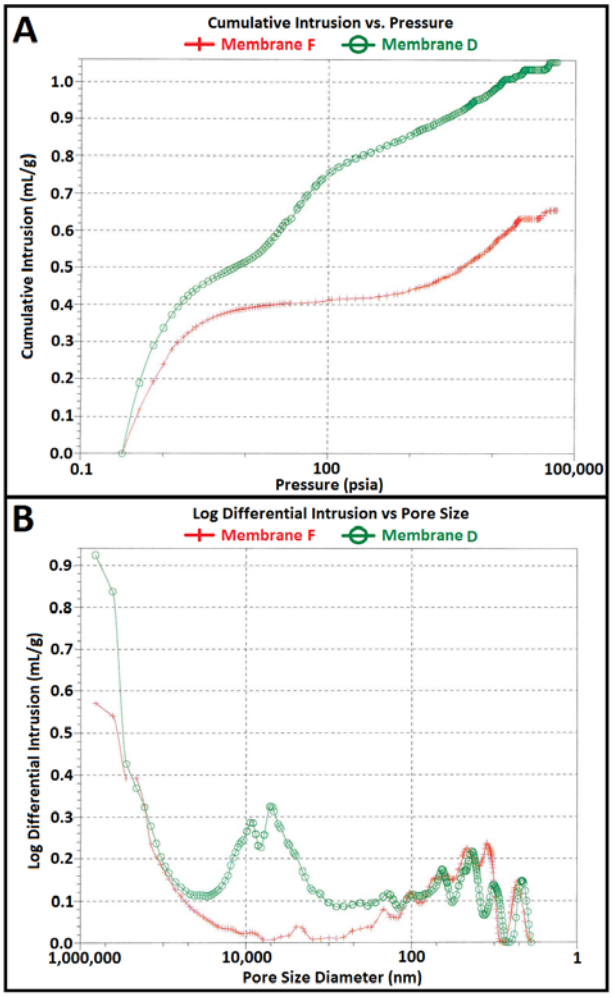

FIG. 4 MEMBRANE D AND MEMBRANE F POROSIMETRY. AS LABELLED IN DIAGRAM.

The apparent changes in porosity with ethanol content should be reflected in the lateral flow rate measured following surfactant treatment. The lateral flow rates were measured for each membrane and plotted in figure 5. The data points show the average flow rate calculated from ten samples at each membrane composition.

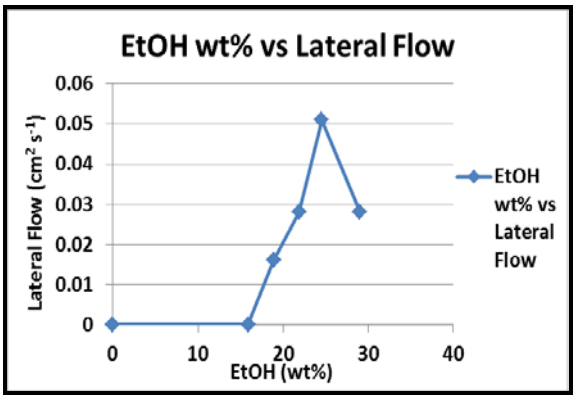

FIG. 2 LATERAL FLOW RATE AGAINST THE ETHANOL CONTENT FOR EACH OF THE MEMBRANES PREPARED HERE.

The control membrane and membrane A showed negligible flow rates in these measurements. However, as the ethanol content in the preparation lacquer rises the flow rate increases through membrane B (avg. 0.0165 cm^2 s^{-1} max. 0.018 cm^2 s^{-1} min. 0.015 cm^2 s^{-1}), membrane C (avg. 0.0282 cm^2 s^{-1} max. 0.031 cm^2 s^{-1} min. 0.026 cm^2 s^{-1}) to a maximum in membrane D (avg. 0.0508 cm^2 s^{-1} max. 0.054 cm^2 s^{-1} min. 0.048 cm^2 s^{-1}) before a decrease with membrane E (avg. 0.0276 cm^2 s^{-1} max. 0.030 cm^2 s^{-1} min. 0.025 cm^2 s^{-1}). The trend in lateral flow rate reflects the changes seen in SEM images and the water needed for cloud point reported in figures 2 and 1 respectively. As it might be expected that membrane D exhibits the highest lateral flow rate and the highest water content in the synthesis lacquer. The decrease in lateral flow seen between D and E can be accounted for directly by the decreased total amount of water present which (as the porogen) reflects the total pore volume. However, although similar amounts of water are used in the formation of membranes A-C, this is not reflected in the lateral flow and indicates that the pore morphology has a strong affect. This probably reflects the changes observed in the SEM images with a progression from 1D to a 3D pore network.

Discussion

There are three issues worthy of detailed discussion here. Firstly, the change in membrane structure observed; secondly, the role of ethanol in the membrane synthesis reaction and, finally, the origin of the nodules formed.

Briefly, in this type of phase inversion synthesis process, the membrane is formed from a single phase, homogeneous solution which on addition of non-solvent becomes a dual phase consisting of a polymer rich region (i.e. polymer and solvent) and a polymer poor region (comprised of the non-solvent; water). The phase separation of these leads to pockets of non-solvent which will form the nascent pores of the final membrane structure, while the surrounding polymer rich phase, upon solvent loss, forms the polymer walls.(T. Young & L. Chen 1995) In this sort of phase inversion process, the membrane is precipitated by a combination of s*pinodal decomposition* (SD) and *nucleation and growth* (NG) (Nunes & Inoue 1996; Chae Park et al. 1999; Pinnau & William J. Koros 1993a). The rate of evaporation is the key to the morphology of the membrane. In general, precipitation occurs because evaporation leads to loss of solvent and de-stabilisation of the polymer rich phase.[24]. If the solvent evaporation is rapid, the evaporation forces bring polymer molecules to the surface increasing their concentration and resulting in skin layers. Further, the 'de-mixing' front passes down through the membrane from the air exposed surface. The rate of solvent evaporation decreases as the demixing front moves back from the air exposed surface and layers of polymer build up above it.(Yiotis, Tsimpanogiannis, Stubos & Yortsos 2006b) This would explain the appearance of the non-ethanol containing membrane. The formation of macrovoids is also a result of rapid solvent evaporation as explained by Kahre et al.[16] Briefly, the interface between the polymer rich and polymer poor phase undergoes motion due to solvent evaporation. Any macrovoid formed by an agglomeration of non-solvent undergoes a differential stress across the leading edge of the void and the trailing edge. This results in convection currents within the voids which in turn promote further non-solvent inclusion and void growth. Ahmad *et al* have argued that macrovoids inhibit lateral flow by increasing the bulk porosity of a membrane without increasing the actual number of pores.(Ahmad et al. 2007) It is also clear that, above a critical size, pores will not contribute to capillary flow. It is suggested that the synthesis of membranes not containing meso-solvent is a direct result of rapid solvent loss. The presence of a skin layer makes imaging macrovoids rather difficult but in membrane A (the lowest ethanol amount used), macrovoids can be clearly seen (Figure 2). Further the direct effect of high evaporation rate related surface stress can be observed on both the macrovoid and microvoid shapes and size.

By using these models, it is possible to explain the results observed here. Acetone has a low boiling point, 50.5°C and a high evaporation rate from the polymer rich component is expected. Although water and acetone are miscible (because of hydrogen bonding), the miscibility of the CN-acetone and water phases is expected to be limited. Thus, evaporative loss from the polymer rich phase is expected to be high. This evaporation results in skin layer formation and production of relatively large macrovoids, as seen in membrane F. As the ethanol content increases it is likely that ethanol can exist in both the polymer rich and polymer deficient phases since the solubility parameter of ethanol and CN are similar. EtOH and acetone mixtures are miscible with no known azeotrope.(Gmehling, Menke, Krafczyk & Fischer 2004a; Gmehling, Menke, Krafczyk & Fischer 2004b) Thus, the boiling point of the solvent in the polymer

rich phase will increase thereby decreasing evaporation rate, then leading to formation of less and smaller sized macrovoids, decreased layer formation and reduced surface strain as seen in the SEM images. At the highest concentration of ethanol, the effect is reduced because the water content of the final mixture is reduced; decreasing total porosity. It is might also be worth speculating about the effect having ethanol in the non-solvent (water) dominated, polymer deficient phase. Ethanol forms an azeotrope with water but this is unlikely to have only a small effect. Its' major effect may be to increase the concentration of CN in this phase, which may reduce the concentration gradient across the phase front and so layering and macrovoid formation are reduced.

These are nodules: spherical morphologies that occur in membranes due to coarsening. The number of these nodules depends on the degree of crystallinity of the membranes. Coarsening occurs when the two separated phases in an *instantaneous* phase inversion build up energy at interfacial regions between the two phases, which makes the solution thermodynamically unstable. Stability is regained by dissipating this energy into coarsening; which is the formation of droplets of semi-crystalline polymer at the interfacial regions. From these droplets, nodules are formed.(Haas & Torkelson 1997) Naturally, the further from instantaneous the phase inversion is, the less coarsening will occur; therefore, if the affinity of the solvent for the non-solvent is increased (as it is through the use of a meso-solvent here), the phase inversion will proceed more through the spinodal region of nucleation and growth (T. Young & L. Chen 1995) and reduce the degree of coarsening and hence the eventual number of nodules.

The formation of nodules observed in the solutions is thought to result from an Ostwald ripening process occurring at the interface of a dispersed phase of the polymer rich and deficient phases.(Pinnau & William J. Koros 1993b; Haas & Torkelson 1997) Given that nodules, like other polymer structures such as epitaxials and spherulites, are crystalline,(Van-de-Witte 1996; Stevens 1999) it is unsurprising that the appearance of the highly crystalline phase is only seen for ethanol containing preparations. It is suggested that the ethanol addition promotes these phases because the ethanol mediates interactions between the polymer rich and polymer poor phases results in higher concentrations of dispersed phases (since the ethanol could stabilise polymer rich phases in the non-solvent). In this way, decreased layering and nodule formation rates are likely to be closely related.

It is tempting, given the morphologies observed in the SEM images, to say that the effect of water upon on the final structure of the membranes is the dominant effect. However, the structure of membrane F in which no ethanol has been in use, while the non-solvent treatment of the casting solution is maintained, shows conclusively that the incorporation of the meso-solvent ethanol is essential to yield the structures that typify membrane D which have greater lateral flow rate.

Conclusion

The inclusion of ethanol in the membrane casting solution at cloud point of CN lateral flow membranes prepared by phase inversion effectively prevents the formation of both skin layers and macrovoids, as shown in SEM cross sectional and surface images and mercury porosimetry data. In addition to the prevention of these undesirable structural anomalies, the inclusion of ethanol also increases the porosity of the CN membrane internal structure as well as lateral flow rates significantly, and the prevalence of nodules in membrane formation; furthermore, these spherical polymer structures remain in the final membrane. Their increased numbers result in an increased crystallinity of the polymer solution, as shown in XRD analysis of the final membranes. The overall conclusion of the work reported here is that all these controlled changes in membrane internal structure are achieved through a reduction in the rate of evaporation of solvent from the membrane air exposed surface/demixing front. The use of a meso-solvent to this end should be applicable to any membrane production process utilizing polymer VIPS and future work will be centred on such investigations.

ACKNOWLEDGMENTS

Dr. Joseph Tobin and Dr. John Hanrahan of Glantreo Ltd., Ireland, Steve Coulsen of Micromeritics, UK, Sean Quilty of Particular Sciences, Ireland, Fred Jones of MCA Services UK, Mark Armstrong of University College Cork, Chemistry Dept. The Science Foundation Ireland and CRANN research grant is also acknowledged for financial support of the work.

REFERENCES

Ahmad, A.L. et al., 2008. Synthesis and Characterization of Polymeric Nitrocellulose Membranes: Influence of

Additives and Pore Formers on the Membrane Morphology. Journal of Applied Polymer Science, 108(4), 2550-2557.

Ahmad, A.L., Low, S. & Shukor, S., 2007. Effects of Membrane Cast Thickness on Controlling the Macrovoid Structure in Lateral Flow Nitrocellulose Membrane and Determination of Its Characteristics. Scripta Materialia, 57(8), 743-746. Available at: http:// linkinghub.elsevier.com/retrieve/pii/S1359646207004514 [Accessed August 23, 2010].

Ahmad, A.L., Sarif, M. & Ismail, S., 2005. Development of an Integrally Skinned Ultrafiltration Membrane for Wastewater Treatment: Effect of Different Formulations of PSf / NMP / PVP on Flux and Rejection. Desalination, 179(November 2004), 257-263.

Arirachakaran, S. et al., 1989. An Analysis of Oil/Water flow Phenomena in Horizontal Pipes. In society of Petroleum Engineers, Oklahoma.

Barton, A.F.M., 1990. CRC Handbook of Polymer-Liquid Interaction Parameters and Solubility Parameters, CRC Press.

Barton, B.F., Reeve, J.L. & McHugh, a. J., 1997. Observations on the Dynamics of Nonsolvent-Induced Phase Inversion. Journal of Polymer Science Part B: Polymer Physics, 35(4), 569-585. Available at: http:// doi.wiley.com/ 10.1002/ (SICI) 1099-0488 (199703)35:4< 569:AID-POLB5>3.0.CO;2-L.

Chae, H. et al., 1999. Membrane Formation by Water Vapor Induced Phase Inversion. Journal of Membrane Science, 156, 169-178.

Chae Park, H. et al., 1999. Membrane Formation by Water Vapor Induced Phase Inversion. Journal of Membrane Science, 156(2), 169-178. Available at: http:// linkinghub.elsevier.com/retrieve/pii/S0376738898003597.

Flynn, E.J. et al., 2012. Unusual Trend of Increasing Selectivity and Decreasing Flux with Decreasing Thickness in Pervaporation Separation of Ethanol/Water Mixtures Using Sodium Alginate Blend Membranes. Journal of Colloid and Interface Science, 370(1), 176-82. Available at: http:// www.ncbi.nlm.nih. gov/pubmed/22261269 [Accessed February 15, 2012].

Gmehling, J., Menke, J., Krafczyk, J. & Fischer, K., 2004a. Azeotropic Data, Volume 1, Wiley-VCH.

Gmehling, J., Menke, J., Krafczyk, J. & Fischer, K., 2004b. Azeotropic Data, Volume 2, Wiley-VCH.

Haas, C.K. & Torkelson, J.M., 1997. Two-Dimensional Coarsening and Phase Separation in Thin Polymer Solution Films. Physical Review E, 55(3), 3191-3201.

Hao, J. & Wang, S., 2001. Calculation of Alcohol-Acetone-Cellulose Acetate Ternary Phase Diagram and their Relevance to Membrane Formation. Jounral of Applied Polymer Science, 80, 1650-1657.

Hu, B. et al., 2006. Investigation of Phase Inversion of Liquid-Liquid Dispersions in Agitated Vessels*. Tsinghua Science & Technology, 11(2), 202-206. Available at: http://linkinghub.elsevier.com/retrieve/ pii/S1007021406701766.

Kang, Y.-S. et al., 1988. The Mechanism of Assymetric Membrane Formation via Phase Inversion. Polymer Society of Korea, 12(3), 279-287.

Khare, V.P. et al., 2002. Macrovoid Growth during Polymer Membrane Casting. Desalination, 145(1-3), 17-23.

Kim, J.-hoon & Lee, K.-ho, 1998. Effect of PEG Additive on Membrane Formation by Phase Inversion. Rain, 138, 153-163.

Lönnberg, M. & Carlsson, J., 2001. Chromatographic Performance of a Thin Microporous Bed of Nitrocellulose. Journal of Chromatography. B, Biomedical Sciences and Applications, 763(1-2), pp.107-20. Available at: http://www.ncbi.nlm.nih.gov/ pubmed /11710569.

Nunes, S.P. & Inoue, T., 1996. Evidence for Spinodal Decomposition and Nucleation and Growth Mechanisms during Membrane Formation. Journal of Membrane Science, 111(1), 93-103.

Pauchard, L. & Allain, C., 2003. Buckling instability Induced by Polymer Solution Drying. Europhysics Letters, 62(6), 897-903.

Paulsen, F.G., Shojaie, S.S. & Krantz, W.B., 1994. Effect of Evaporation Step on Macrovoid Formation in Wet-Cast Polymeric Membranes. Journal of Membrane Science, 91(3), 265-282.

Pesek, S.C. & Koros, W.J., 1993. Aqueous Quenched Asymmetric Polysulfone Membranes Prepared by Dry/Wet Phase Separation. Journal of Membrane Science, 81(1-2), 71-88.

Pinnau, I. & Koros, William J., 1993a. A Qualitative Skin Layer Formation Mechanism for Membranes Made by

Dry/Wet Phase Inversion. Journal of Polymer Science Part B: Polymer Physics, 31(4), 419-427. Available at: http://doi.wiley.com/10.1002/polb.1993.090310406.

Pinnau, I. & Koros, William J., 1993b. A Qualitative Skin Layer Formation Mechanism for Membranes Made by Dry/Wet Phase Inversion. Journal of Polymer Science Part B: Polymer Physics, 31(4), 419-427.

Salamone, J.P., 1996. Polymeric Materials Encyclopedia Vol. 6, CRC Press.

Smolders, C.A. et al., 1992. Microstructures in phase-Inversion Membranes. Part 1. Formation of Macrovoids. Journal of Membrane Science, 73(2-3), 259-275.

Stevens, M.P., 1999. Chapter 3: Chemical Structure and Polymer Morphology. In Polymer Chemistry: An Introduction. Oxford University Press, Inc., pp. 61-95.

Thurn-Albrecht, T. et al., 2004. Semicrystalline Morphology in Thin Films of Poly (3-Hexylthiophene). Colloid & Polymer Science, 282(8), 932-938. Available at: http://www.springerlink.com/openurl.asp?genre=article&id=doi:10.1007/s00396-004-1100-9 [Accessed July 27, 2012].

Ulbricht, M., 2006. Advanced Functional Polymer Membranes. Polymer, 47(7), 2217-2262. Available at: http://linkinghub.elsevier.com/retrieve/pii/S0032386106001303.

Van-de-Witte, P., 1996. Phase Separation Processes in Polymer Solutions in Relation to Membrane Formation. Journal of Membrane Science, 117(1-2), 1-31.

Vandewitte, P. et al., 1996. Phase Separation Processes in Polymer Solutions in Relation to Membrane Formation. Journal of Membrane Science, 117(1-2), 1-31. Available at: http://linkinghub.elsevier.com/retrieve/pii/0376738896000889.

Yiotis, A.G., Tsimpanogiannis, I.N., Stubos, A.K. & Yortsos, Y.C., 2006a. Pore-network Study of the Characteristic Periods in the Drying of porous Materials. Journal of Colloid and Interface Science, 297(2), 738-48. Available at: http://www.ncbi.nlm.nih.gov/pubmed/ 16359693 [Accessed August 3, 2010].

Yiotis, A.G., Tsimpanogiannis, I.N., Stubos, A.K. & Yortsos, Y.C., 2006b. Pore-Network Study of the Characteristic Periods in the Drying of Porous Materials. Journal of colloid and interface science, 297(2), 738-48. Available at: http://www.ncbi.nlm.nih.gov/pubmed/ 16359693 [Accessed August 3, 2010].

Yip, Y. & Mchugh, a, 2006. Modeling and Simulation of Nonsolvent Vapor-Induced Phase Separation. Journal of Membrane Science, 271(1-2), 163-176. Available at: http://linkinghub.elsevier.com/retrieve/pii/S0376738805005533 [Accessed August 9, 2010].

Young, T. & Chen, L., 1995. Pore Formation Mechanism of Membranes from Phase Inversion Process. Desalination, 103(3), 233-247. Available at: http://linkinghub.elsevier.com/retrieve/pii/0011916495000763.

Young, T.-H. & Chen, L.-W., 1995. Pore Formation Mechanism of Membranes from Phase Inversion Process. Desalination, 103, 233-247.